How to cite: Angew. Chem. Int. Ed. 2023, e202305977
doi.org/10.1002/anie.202305977

Metal-Organic Frameworks Hot Paper

A Humidity-Induced Large Electronic Conductivity Change of 10^7 on a Metal-Organic Framework for Highly Sensitive Water Detection

*Wei-Hua Deng, Qiao-Hong Li, Jie Chen, Chuan-Zhe Wang, Zhi-Hua Fu, Xiao-Liang Ye, Guan-E Wang, and Gang Xu**

Abstract: The electronic conductivity (EC) of metal–organic frameworks (MOFs) is sensitive to strongly oxidizing guest molecules. Water is a relatively mild species, however, the effect of H_2O on the EC of MOFs is rarely reported. We explored the effect of H_2O on the EC in the MOFs $(NH_2)_2$-MIL-125 and its derivatives with experimental and theoretical investigations. Unexpectedly, a large EC increase of 10^7 on H_2SO_4@-$(NH_2)_2$-MIL-125 by H_2O was observed. Brønsted acid–base pairs formed with the $-NH_2$ groups, and H_2SO_4 played an important role in promoting the charge transfer from H_2O to the MOF. Based on H_2SO_4@-$(NH_2)_2$-MIL-125, a high-performance chemiresistive humidity sensor was developed with the highest sensitivity, broadest detection range, and lowest limit of detection amongst all reported sensing materials to date. This work not only demonstrated that H_2O can remarkably influence the EC of MOFs, but it also revealed that post-modification of the structure of MOFs could enhance the influence of the guest molecule on their EC to design high-performance sensing materials.

The electronic conductivity (EC) in metal–organic frameworks (MOFs) has aroused enormous research interest.[1] The unique combination of their microporous structure and electronic properties may open intriguing applications, such as in electrocatalysis, energy storage, voltage-gated ion channels, liquid-gated field-effect transistors and various chemical sensors.[2] The penetrable structures, large surface area and accessible open-metal sites/functional groups sometimes make the conduction of MOFs highly susceptible to guest molecules. The embedment of foreign molecules in MOFs results in large regulations in their conductivity.[3] In these studies, foreign molecules with relatively high redox activity, such as I_2 (0.54 V vs *NHE*) or 7, 7, 8, 8-tetracyanoquinodimethane (TCNQ, 0.37 V vs *NHE*), have been commonly used.[4] Compared with these molecules, H_2O has relatively mild activity (redox potential of −0.83 V vs *NHE*).[5] It exists in the air with high concentration (1.4×10^4 ppm at 50 % relative humidity (RH)). Meanwhile, H_2O has been reported to promote electron transfer (ET) in biological systems, such as covalently cross-linked azurin complexes, the hydroxylating domain of peptidyl glycine a-amidylating monooxygenase, DNA and enzyme subunits.[6] In these systems, H_2O facilitates ET by forming ET coupling pathways, mediating electron tunneling rates and lowering the activation-free energies for ET.[6a,b,d,7] In biological systems, H_2O-mediated ET has also been intensively studied in materials for geochemistry, electrochemistry, photocatalysis and sensors. Many MOFs were reported to adsorb a large amount of water even at a low RH range.[8] However, the reported studies on the humidity-dependent conductivity of MOFs exclusively focused on proton rather than electron conduction.[9] Given that (1) H_2O plays an important role in promoting ET in various applications and (2) H_2O is ubiquitous in the environment and easily adsorbed by MOFs during the preparation, storage and application processes, the influence of H_2O on the electronic conduction of MOFs should be revealed.[10]

In this work, for the first time, the influence of H_2O on the electronic conduction of a series of representative MOFs, MIL-125, $(NH_2)_2$-MIL-125 and H_2SO_4@$(NH_2)_2$-MIL-125, was explored. An unexpected large regulation in their electronic conduction with a value as high as seven orders of magnitude was observed by the DC Wagner's polarization technique. The possible mechanism for this phenomenon was revealed by combining experimental and theoretical studies. Moreover, a high-performance chemiresistive humidity sensor was developed based on the large influence of H_2O on the conductivity of H_2SO_4@$(NH_2)_2$-MIL-125. Compared with the reported humidity sensing materials, it reached the highest sensitivity, the lowest experimental limit of detection (LOD), large detection range, high selectivity and excellent long-term stability.

[*] Dr. W.-H. Deng, Prof. Q.-H. Li, J. Chen, C.-Z. Wang, Dr. Z.-H. Fu, Dr. X.-L. Ye, Prof. G.-E Wang, Prof. G. Xu
State Key Laboratory of Structural Chemistry, Fujian Provincial Key Laboratory of Materials and Techniques toward Hydrogen Energy, Fujian Institute of Research on the Structure of Matter, Chinese Academy of Sciences
Fuzhou, Fujian, 350002 (China)
E-mail: gxu@fjirsm.ac.cn

Dr. W.-H. Deng
Fujian Provincial Key Laboratory of Polymer Materials, College of Chemistry and Materials Science, Fujian Normal University
<350117 Fuzhou (China)

Prof. G. Xu
Fujian Science & Technology Innovation Laboratory for Optoelectronic Information of China
Fuzhou, Fujian 350108 (China)
and
University of Chinese Academy of Sciences
Beijing 100049 (China)

Herein, a series of robust titanium MOFs, $(NH_2)_x$-MIL-125 ($x=0$, 1, 2) nanoflakes, were synthesized with the molecular formula $Ti_8O_8(OH)_4$-($(NH_2)_x$-BDC)$_6$ (for details, see Supporting Information).[11] MIL-125 had a 3D porous structure that is constructed by the connection of octahedral and tetrahedral cages (Figure S1).[12] These cages were formed by the coordination of 1,4-benzene dicarboxylates (H_2-BDC) with Ti-oxo clusters ($Ti_8O_{20}(OH)_4$). The diameter of their free cavities was in the range of 5–7 Å, into which water molecules can be easily captured and concentrated into the cages.[12] NH_2-MIL-125 and $(NH_2)_2$-MIL-125 are iso-structures of MIL-125 and possess one or two uncoordinated $-NH_2$ groups on the benzene ring of their frameworks, respectively.[13] Moreover, the framework possesses a permanent high porosity and high density of hydrophilic active sites (titanium oxo clusters, free $-NH_2$ and carboxylate groups) for the uptake of large amounts of water molecules at low-pressure regions.

The SEM image of $(NH_2)_2$-MIL-125 showed a large-scale version of homogeneous nanoplates (Figure S2a). After H_2SO_4 treatment, the resultant H_2SO_4@$(NH_2)_2$-MIL-125 had a similar morphology (Figure S2b). As shown in Figure 1a and Table S1, the chemical composition of H_2SO_4@$(NH_2)_2$-MIL-125 was confirmed by Fourier transform infrared (FT-IR) spectroscopy (hydrogen-bonded sulfate anions at 1063 cm^{-1}),[14] inductively coupled plasma atomic emission spectroscopy (ICP-AES), elemental analysis (EA) and dry method analysis. On the basis of the ICP-AES and EA results, the H_2SO_4 content could be estimated at 21.6 wt %, which was in line with that obtained by the dry method analysis (22.5 wt %, see the experimental section for detailed information). The N/S atom ratio was 2.3, indicating that each $-NH_2$ group bonded with 0.44 H_2SO_4.

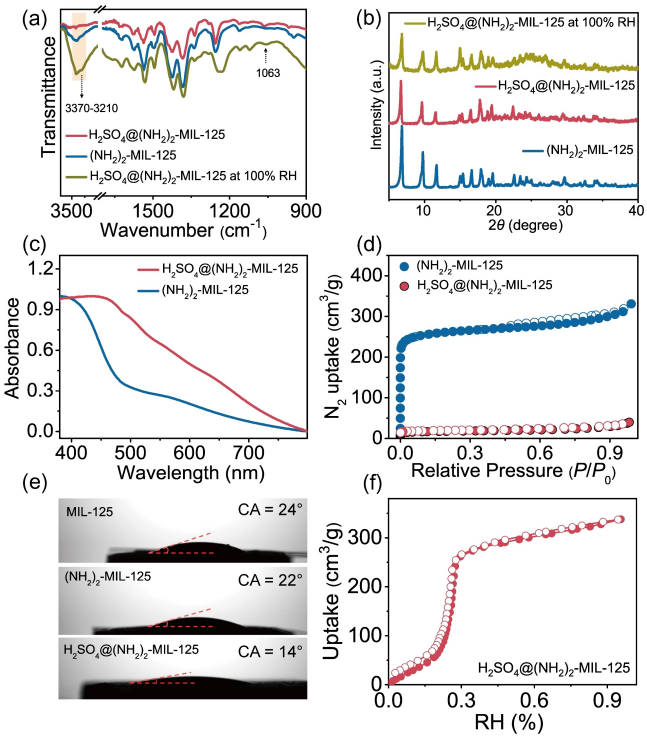

Figure 1. a) FT-IR spectra; b) PXRD patterns; c) UV-vis absorption spectra; d) N_2 adsorption-desorption isotherms at 77 K; e) Water contact angle measurements; f) Water adsorption-desorption isotherm of H_2SO_4@$(NH_2)_2$-MIL-125 at 298 K of MIL-125, $(NH_2)_2$-MIL-125, H_2SO_4@$(NH_2)_2$-MIL-125, and H_2SO_4@$(NH_2)_2$-MIL-125 at 100% RH.

The PXRD patterns of H_2SO_4@$(NH_2)_2$-MIL-125 coincided with those of $(NH_2)_2$-MIL-125, thereby demonstrating that the crystal structure was retained after acid treatment.[15] The diffraction peaks of H_2SO_4@$(NH_2)_2$-MIL-125 were sharp after exposure to 100 % RH for 72 h, which displayed its good water stability (Figure 1b). Compared with that of $(NH_2)_2$-MIL-125, the UV-vis absorption of H_2SO_4@$(NH_2)_2$-MIL-125 showed an extra absorption band ranging from 520 to 720 nm (Figure 1c). This result demonstrated the formation of Brønsted acid–base pairs between $-NH_2$ groups and H_2SO_4.[14a] After H_2SO_4 treatment, the peak of $-NH_2$ groups of $(NH_2)_2$-MIL-125 at 3370–3210 cm^{-1} in FT-IR become weaker (Figure 1a), and the peaks of C–N, –NH and $-NH_2$ in the XPS spectra exhibited a significant shift (Figures S3–4). These results further confirmed the strong interaction between sulfuric acid and amino groups.

N_2 sorption measurements at 77 K revealed the microporous structure of $(NH_2)_2$-MIL-125 (Figure 1d). After H_2SO_4 treatment, its Brunauer–Emmett–Teller surface area decreased from 913 to 64 $m^2 g^{-1}$. These results confirmed the successful impregnation of H_2SO_4. To estimate the hydrophilicity of MIL-125, $(NH_2)_2$-MIL-125 and H_2SO_4@$(NH_2)_2$-MIL-125, the water contact angles were measured at RT. As shown in Figure 1e, the initial contact angles of MIL-125, $(NH_2)_2$-MIL-125 and H_2SO_4@-$(NH_2)_2$-MIL-125 were ≈24°, 22° and 14°, respectively, which demonstrated the highly hydrophilic nature of these samples. The $-NH_2$ group and H_2SO_4 could further improve hydrophilicity.

The water sorption isotherm of H_2SO_4@$(NH_2)_2$-MIL-125 was measured at 298 K (Figure 1f), and the water uptake was calculated as several water molecules per unit cell of H_2SO_4@$(NH_2)_2$-MIL-125 (n/unit cell). The overall water adsorption isotherm exhibited an S-shaped profile. It revealed an initial uptake of 48 water molecules per unit cell at low humidity (≤10 % RH). When increasing RH to 30 %, the water uptake sharply increased to 423 water molecules per unit cell. Subsequently, water uptake slowed down and the maximum uptake was 547 water molecules per unit cell at 95 % RH. The different adsorption amounts between N_2 and H_2O are commonly observed in other MOFs and may be attributed to (1) the different dynamic aperture sizes of the pores in H_2SO_4@$(NH_2)_2$-MIL-125 at different temperatures (N_2 at 77 K and H_2O at 298 K),[16] (2) H_2O with a smaller kinetic diameter of 2.6 Å than N_2 with a larger kinetic diameter of 3.6 Å.[17] After exposing H_2SO_4@$(NH_2)_2$-MIL-125 to 100 % RH, the peaks at 1535 (C=O), 1421 (–(O–C–O)–) and 1380 cm^{-1} (C–N) in the FT-IR spectra shifted, which demonstrated the strong interaction between H_2O and $-NH_2$/carboxylate groups (Figure 1a).

There are two kinds of charge carriers in H_2SO_4@-$(NH_2)_2$-MIL-125, namely, ions and electrons. The contribution of these charge carriers to the total current could be revealed by the direct current (DC) Wagner's polarization technique.[18] $\mathbf{I_t}$ is a sum of the electron current ($\mathbf{I_e}$) and the proton current ($\mathbf{I_{ion}}$). $\mathbf{t_e}$, the electronic transference number, was defined as the ratio of $\mathbf{I_e}$ to $\mathbf{I_t}$, which quantitatively identified the extent of electronic contribution to the total current of H_2SO_4@$(NH_2)_2$-MIL-125. H_2SO_4@$(NH_2)_2$-MIL-125 powder particles were prepared into a thick film and then connected by two Pt wires as electrodes (Figure S5). At the moment of applying a DC voltage across the film, the current is $\mathbf{I_t}$. However, the Pt electrode would block the proton whilst allowing the electron to pass. Thus, $\mathbf{I_t}$ would decrease with time increment due to the disappearance of $\mathbf{I_{ion}}$ and finally reached a steady state with pure $\mathbf{I_e}$. RH-dependent DC of the H_2SO_4@$(NH_2)_2$-MIL-125 film was monitored as a function of time at 1 V and 25 °C (Figure 2a).

The following results were obtained: (1) $\mathbf{I_t}$ and $\mathbf{I_e}$ were enhanced with increasing RH, indicating that water molecules could increase the concentration of ions and electrons (Figure 2b). (2) $\mathbf{t_e}$ showed a non-linear relationship with RH (Figure 2c). At dry air (≈0 % RH), $\mathbf{I_e}$ was only 1.4×10^{-13} A and $\mathbf{t_e}$ was ≈2 %, indicating negligible EC. When RH increased to 20 %, $\mathbf{I_e}$ sharply increased by $\approx5\times10^5$ times, and $\mathbf{t_e}$ increased from 2 % to 67 %. This result indicated that the adsorbed H_2O molecules mainly increased EC at low RH. At 10 % RH, $\mathbf{t_e}$ peaked at 75 % and then gradually decreased with the increase in humidity. At a high RH, H_2O molecules increased the proton conductivity. Meanwhile, $\mathbf{I_e}$ monotonously increased with the increase in RH, and finally, $\mathbf{I_e}$ of H_2SO_4@$(NH_2)_2$-MIL-125 varied by 10^7 times from 0 % to 100 % RH and reached 3.9×10^{-6} A. Notably, we first observed the increase of water-induced large electron conduction by 10^7 times on a MOF. H_2O possessed the lower redox potentials compared with oxidative guest molecules (e.g. MV^{2+}, TCNQ and I_2) or conducting polymers (e.g. PEDOT) used to tune the conductivity of MOFs (Figure 2d). These results demonstrated that mild molecules, such as the water molecule, could remarkably fluctuate the EC of MOFs.

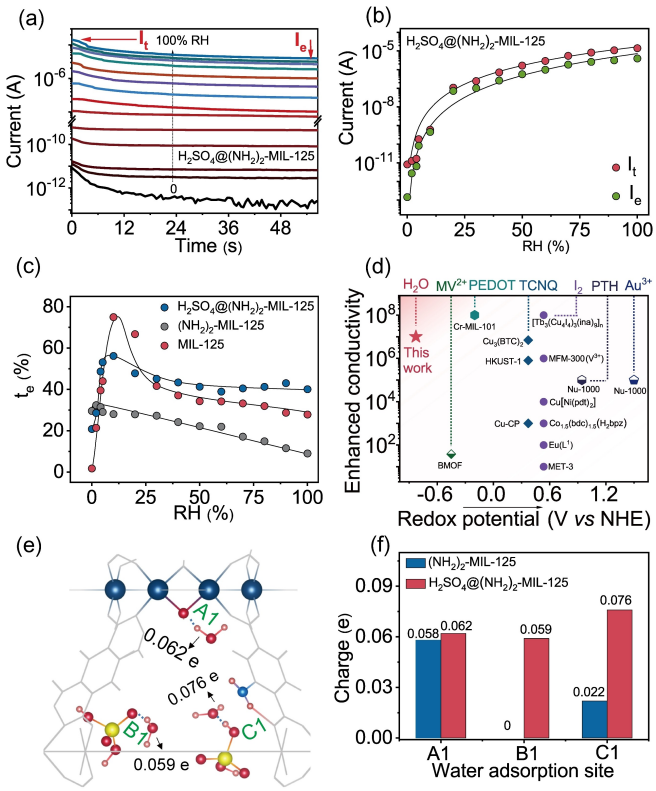

Figure 2. a) Curves of current vs. time of H_2SO_4@$(NH_2)_2$-MIL-125 obtained by the DC Wagner's polarization technique. b) RH dependent $\mathbf{I_e}$ and $\mathbf{I_t}$ of H_2SO_4@$(NH_2)_2$-MIL-125 deduced from (a). c) RH dependent $\mathbf{t_e}$ of MIL-125, $(NH_2)_2$-MIL-125, and H_2SO_4@$(NH_2)_2$-MIL-125. d) Comparison of the conductivities of MOFs obtained via different redox-active guest molecules or conducting polymer (MV^{2+}: cationic methyl viologen; PEDOT: poly-ethylenedioxythiophene). e), f) Atomic partial charges of water adsorbed at A1/B1/C1 sites of H_2SO_4@$(NH_2)_2$-MIL-125 and $(NH_2)_2$-MIL-125, respectively, by DFT-D calculation.

To reveal more details, the time-dependent DC of MIL-125 and $(NH_2)_2$-MIL-125 was also measured (Figure S6). In the range of 0–20 % RH, $\mathbf{I_e}$ of MIL-125 and $(NH_2)_2$-MIL-125 increased by 38 and 4.3×10^3 times, respectively, which are much smaller than that of H_2SO_4@$(NH_2)_2$-MIL-125. Meanwhile, the $\mathbf{t_e}$ values of MIL-125 and $(NH_2)_2$-MIL-125 at 10 % RH were 28 % and 56 %, respectively, which were also smaller than that of H_2SO_4@$(NH_2)_2$-MIL-125. These results clarified that $-NH_2$ and H_2SO_4 in the structure played a critical role in promoting H_2O-enhanced EC. Increasing the RH > 10 %, $\mathbf{I_{ion}}$ increased and became dominant in charge transport, resulting in decreased $\mathbf{t_e}$. Compared with MIL-125 and $(NH_2)_2$-MIL-125, H_2SO_4@-$(NH_2)_2$-MIL-125 showed a more obvious decrease in $\mathbf{t_e}$. This was because H_2SO_4@$(NH_2)_2$-MIL-125 could provide higher $\mathbf{I_{ion}}$ due to the dissociation of guest H_2SO_4.

Density functional theory (DFT) calculation, which DFT-D correction was used for weak interaction, was performed to further elucidate the mechanism of electron transport in the H_2O/H_2SO_4@$(NH_2)_2$-MIL-125 system (Figure S7, see the Supporting Information for details).[19] The adsorption sites of water molecules on H_2SO_4@$(NH_2)_2$-MIL-125 were confirmed and are shown in Figure S8. The most stable H_2O adsorption site, A1, was in the middle of the TiO_x ring. It was constructed by hydrogen bond interaction with O atoms of the TiO_x ring and had an adsorption energy of −1.23 eV (Figure S8a). The second stable H_2O adsorption site, B1, was stabilized by hydrogen bond interaction with H_2SO_4 (Figure S8b) and had an adsorption energy of −0.96 eV. The third stable adsorption site, C1 (Figure S8c), was between the H_2SO_4 and $-NH_2$ groups. It was stabilized by hydrogen bond interaction with H_2SO_4 and $-NH_2$ and had an adsorption energy of −0.70 eV. To further verify the influence of H_2O on its conductivity, the atomic partial charges of water-adsorbed sites of H_2SO_4@$(NH_2)_2$-MIL-125 and $(NH_2)_2$-MIL-125 were calculated (see Figures 2e and f and Table S2 for details). We found that 0.062/0.059/0.076 electrons transferred from each adsorbed water at the A1/B1/C1 sites to H_2SO_4@-

$(NH_2)_2$-MIL-125, respectively. In 10 % RH atmosphere, one unit cell of H_2SO_4@$(NH_2)_2$-MIL-125 adsorbed 48 water molecules (Figure 1f), which should provide considerable electrons to enhance conductivity. $(NH_2)_2$-MIL-125 had only the A1 site in the middle of the TiO_x ring and a similar C1 site but without the hydrogen bond interaction with H_2SO_4. Moreover, the A1 and C1 sites at $(NH_2)_2$-MIL-125 only transferred 0.057 and 0.024 electrons, respectively, which were less than those at H_2SO_4@$(NH_2)_2$-MIL-125. These results revealed the important role of H_2SO_4 in prompting the ET from adsorbed water to MOFs.

Chemiresistive sensing materials with a experimentally reached LOD lower than 5 % RH (1570 ppm at 25 °C) for H_2O are rare, and those with experimental LOD lower than 0.3 % RH (94 ppm at 25 °C) has never been reported yet.[20] The large change of humidity to the EC of H_2SO_4@$(NH_2)_2$-MIL-125 inspired us to develop a highly sensitive humidity sensing material. The sensor was developed by drop-casting the methanol suspension of H_2SO_4@$(NH_2)_2$-MIL-125 onto the interdigital electrodes of an Al_2O_3 substrate. The linear *I–V* curve indicated good ohmic contact between the samples and electrodes (Figure S9). The sensing performances were measured with a home-made setup, and the concentration of H_2O in the analyte flow was calibrated by a commercial instrument (details see Supporting Information, Figures S10–11). The H_2O sensing performance of H_2SO_4@$(NH_2)_2$-MIL-125 was evaluated at room temperature (RT) (Figure 3a, b). When circularly exposed to dry air and humidity, H_2SO_4@$(NH_2)_2$-MIL-125 showed a dynamic response and recovery to H_2O. Notably, this material could respond to the concentration from 0.06 % to 100 % RH (20 to 3.2×10^4 ppm), which was the broadest detection range in the reported chemiresistive sensing materials (Figure 4a and Table S3). H_2SO_4@$(NH_2)_2$-MIL-125 also possessed the highest sensitivity in the whole RH range and all reported materials (Figure 4b and Table S3). Typically, it had responses of 1.6×10^3, 2.3×10^7 and 1.2×10^8 at 5 %, 50 % and 90 % RH, respectively. These values were 800, 3800 and 2000 times higher than those of the reported best sensing materials (Table S3). It could also experimentally respond to 0.06 % RH (20 ppm) H_2O, which represented a LOD that was 60 times lower than the reported lowest detected humidity (Table S3).

H_2SO_4@$(NH_2)_2$-MIL-125 demonstrated unique selectivity to H_2O and had a selectivity factor ($R_{humidity}/R_{interference}$) as high as 13 to the strongest commonly existing 13 interferences, including acetone, ethanol, methanol, SO_2, H_2, NH_3, CO_2, benzene, toluene, CH_4, CH_3–CH_3, CH_2=CH_2 and CH≡CH (Figures 3c-top, S12, S13). The response and recovery time of H_2SO_4@$(NH_2)_2$-MIL-125 were 4.8 and 0.3 min, respectively (inset in Figure 3b). H_2SO_4@$(NH_2)_2$-MIL-125 toward 5 % RH was examined for seven successive assays (Figure S14). The coefficient of variation (CV) was as low as 6.7 %, indicating its good response repeatability. The fabricated device was tested for over 8 months. There was almost no variety in its response to 5 % RH, suggesting its excellent long-term stability (Figure 3c-down). The humidity performance increased in the sequence of MIL-125, NH_2-MIL-125, $(NH_2)_2$-MIL-125 and H_2SO_4@$(NH_2)_2$-MIL-125 (Figures 3d and S15, S16). These experiments suggested that –NH_2 groups and H_2SO_4 on H_2SO_4@$(NH_2)_2$-MIL-125 were critical for high sensing performance.

In summary, for the first time, the influence of H_2O on the EC of MOF materials was revealed. Unexpectedly, a profound regulation as high as 10^7 times on the EC of a representative MOF, H_2SO_4@$(NH_2)_2$-MIL-125, was observed. Experimental and theoretical calculations clarified that the Brønsted acid–base pairs that formed between the

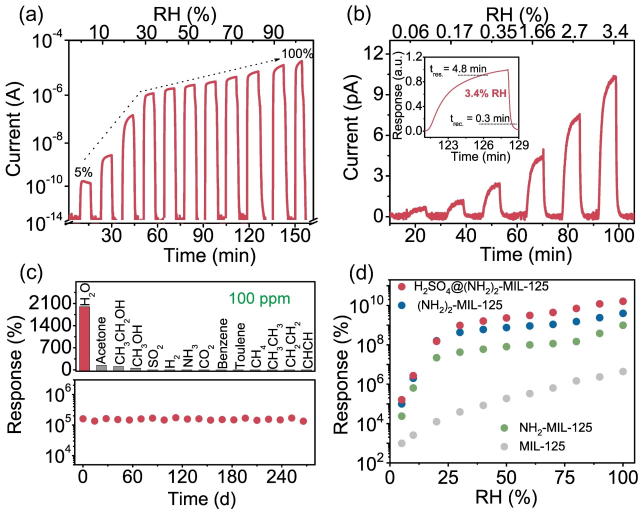

Figure 3. Real-time dynamic response-recovery curves of H_2SO_4@$(NH_2)_2$-MIL-125 to water in the concentration range of a) 5–100 % RH, and b) 0.06–3.4 % RH (inset in (b): response and recovery time to 3.4 % RH). c-up) Selectivity analysis (100 ppm for all analytes), and c-down) long-term stability analysis of H_2SO_4@$(NH_2)_2$-MIL-125. d) Response comparison of MIL-125, NH_2-MIL-125, $(NH_2)_2$-MIL-125 and H_2SO_4@$(NH_2)_2$-MIL-125 under different RH.

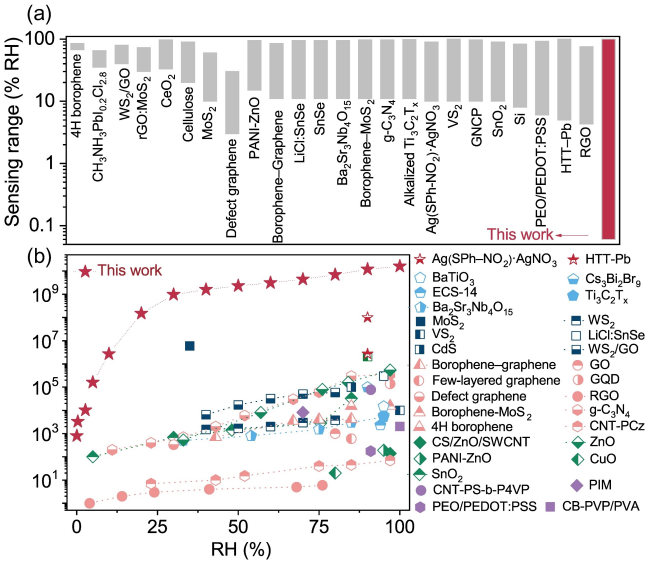

Figure 4. Comparison of humidity performance to state-of-the-art RT humidity chemiresistors: a) Sensing range. b) Response value.

$-NH_2$ group and H_2SO_4 played an important role in promoting the charge transfer from H_2O to $(NH_2)_2$-MIL-125 and resulted in large changes in the EC. According to this result, a highly sensitive chemiresistive humidity sensing material was developed with H_2SO_4@$(NH_2)_2$-MIL-125. It had responses of 800, 3800 and 2000 times higher than those of the reported best sensing materials at 5 %, 50 % and 90 % RH, respectively. It could also experimentally respond to 0.06 % RH (20 ppm) H_2O, which represented a LOD 60 times lower than the reported lowest detected humidity. Moreover, it had the broadest detection range (0.06 % to 100 % RH) reported so far, high selectivity to H_2O amongst 13 commonly existing inference gases/vapors, fast response and recovery speed and excellent long-term stability. This work not only answers the question whether H_2O, a molecule with weak oxidation nature that widely exists in the atmosphere, can influence the EC of MOFs, but it also provides a highly sensitive and selective sensing material for non-contact and real-time detection of ppm-level trace H_2O.

Acknowledgements

This work was financially supported by the National Natural Science Foundation of China (91961115, 62227815, 22171263, 22175176, and 22271281), Scientific Research and Equipment Development Project of CAS (YJ-KYQ20210024), Fujian Science & Technology Innovation Laboratory for Optoelectronic Information of China (2021ZR101), Self-deployment Project Research Program of Haixi Institutes, Chinese Academy of Sciences, CXZX-2022-GH09 and the Natural Science Foundation of Fujian Province (2020J01109, 2021J02017, 2022J05088 and 2022J06032).

Conflict of Interest

The authors declare no conflict of interest.

Data Availability Statement

The data that support the findings of this study are available from the corresponding author upon reasonable request.

Keywords: Electrical Devices · Gas Sensing · Metal–Organic Frameworks · Thin Films · Trace Water Detection

[1] a) X. Chen, J. Dong, K. Chi, L. Wang, F. Xiao, S. Wang, Y. Zhao, Y. Liu, *Adv. Funct. Mater.* **2021**, *31*, 2102855; b) Y. Liu, Y. Wei, M. Liu, Y. Bai, X. Wang, S. Shang, J. Chen, Y. Liu, *Angew. Chem. Int. Ed.* **2021**, *60*, 2887–2891; c) J.-H. Dou, M. Q. Arguilla, Y. Luo, J. Li, W. Zhang, L. Sun, J. L. Mancuso, L. Yang, T. Chen, L. R. Parent, *Nat. Mater.* **2021**, *20*, 222–228; d) T. Panda, R. Banerjee, *Proc. Natl. Acad. Sci. India Sect. A* **2014**, *84*, 331–336; e) F. Gándara, F. J. Uribe-Romo, D. K. Britt, H. Furukawa, L. Lei, R. Cheng, X. Duan, M. O'Keeffe, O. M. Yaghi, *Chem. Eur. J.* **2012**, *18*, 10595–10601.

[2] a) D. Feng, T. Lei, M. R. Lukatskaya, J. Park, Z. Huang, M. Lee, L. Shaw, S. Chen, A. A. Yakovenko, A. Kulkarni, *Nat. Energy* **2018**, *3*, 30–36; b) P. Li, B. Wang, *Isr. J. Chem.* **2018**, *58*, 1010–1018.

[3] S. Jung, L. Huelsenbeck, Q. Hu, S. Robinson, G. Giri, *ACS Appl. Mater. Interfaces* **2021**, *13*, 10202–10209.

[4] a) Y. Jiang, I. Oh, S. H. Joo, Y.-S. Seo, S. H. Lee, W. K. Seong, Y. J. Kim, J. Hwang, S. K. Kwak, J.-W. Yoo, *J. Am. Chem. Soc.* **2020**, *142*, 18346–18354; b) M. Wang, M. Wang, H.-H. Lin, M. Ballabio, H. Zhong, M. Bonn, S. Zhou, T. Heine, E. Canovas, R. Dong, *J. Am. Chem. Soc.* **2020**, *142*, 21622–21627.

[5] D. De Leeuw, M. Simenon, A. Brown, R. Einerhand, *Synth. Met.* **1997**, *87*, 53–59.

[6] a) T. Hayashi, A. Stuchebrukhov, *J. Electroanal. Chem.* **2011**, *660*, 356–359; b) J. Lin, I. A. Balabin, D. N. Beratan, *Science* **2005**, *310*, 1311–1313; c) T. Ramasarma, D. Vaigundan, *Mol. Cell. Biochem.* **2019**, *453*, 197–203; d) L. Xiang, P. Zhang, C. Liu, X. He, H. B. Li, Y. Li, Z. Wang, J. Hihath, S. H. Kim, D. N. Beratan, *Matter* **2020**, *3*, 166–179.

[7] A. Migliore, S. Corni, R. Di Felice, E. Molinari, *J. Phys. Chem. B* **2007**, *111*, 3774–3781.

[8] a) H. Kim, S. Yang, S. R. Rao, S. Narayanan, E. A. Kapustin, H. Furukawa, A. S. Umans, O. M. Yaghi, E. N. Wang, *Science* **2017**, *356*, 430–434; b) J. Canivet, A. Fateeva, Y. Guo, B. Coasne, D. Farrusseng, *Chem. Soc. Rev.* **2014**, *43*, 5594–5617; c) N. C. Burtch, H. Jasuja, K. S. Walton, *Chem. Rev.* **2014**, *114*, 10575–10612; d) A. Cadiau, Y. Belmabkhout, K. Adil, P. M. Bhatt, R. S. Pillai, A. Shkurenko, C. Martineau-Corcos, G. Maurin, M. Eddaoudi, *Science* **2017**, *356*, 731–735; e) N. Hanikel, M. S. Prévot, O. M. Yaghi, *Nat. Nanotechnol.* **2020**, *15*, 348–355; f) K. Onda, B. Li, J. Zhao, K. D. Jordan, J. Yang, H. Petek, *Science* **2005**, *308*, 1154–1158.

[9] a) K. Otsubo, S. Nagayama, S. Kawaguchi, K. Sugimoto, H. Kitagawa, *JACS Au* **2022**, *2*, 109–115; b) Y. Ye, L. Gong, S. Xiang, Z. Zhang, B. Chen, *Adv. Mater.* **2020**, *32*, 1907090; c) S. C. Sahoo, T. Kundu, R. Banerjee, *J. Am. Chem. Soc.* **2011**, *133*, 17950–17958; d) T. Panda, T. Kundu, R. Banerjee, *Chem. Commun.* **2013**, *49*, 6197–6199.

[10] a) Y. Fuma, M. Ebihara, S. Kutsumizu, T. Kawamura, *J. Am. Chem. Soc.* **2004**, *126*, 12238–12239; b) Y. Kimura, Y. Yoshida, M. Maesato, H. Kitagawa, *Chem. Lett.* **2021**, *50*, 439–441.

[11] W.-H. Deng, P. N. Kumar, W.-H. Li, C. Kashi, M.-S. Yao, G.-D. Wu, G. Xu, *Inorg. Chim. Acta* **2020**, *502*, 119317.

[12] M. Dan-Hardi, C. Serre, T. Frot, L. Rozes, G. Maurin, C. Sanchez, G. Férey, *J. Am. Chem. Soc.* **2009**, *131*, 10857–10859.

[13] a) C. H. Hendon, D. Tiana, M. Fontecave, C. M. Sanchez, L. D'arras, C. Sassoye, L. Rozes, C. Mellot-Draznieks, A. Walsh, *J. Am. Chem. Soc.* **2013**, *135*, 10942–10945; b) Y. Fu, D. Sun, Y. Chen, R. Huang, Z. Ding, X. Fu, Z. Li, *Angew. Chem. Int. Ed.* **2012**, *51*, 3364–3367.

[14] a) S. S. Nagarkar, S. M. Unni, A. Sharma, S. Kurungot, S. K. Ghosh, *Angew. Chem. Int. Ed.* **2014**, *53*, 2638–2642; b) F. Yang, G. Xu, Y. Dou, B. Wang, H. Zhang, H. Wu, W. Zhou, J.-R. Li, B. Chen, *Nat. Energy* **2017**, *2*, 877–883; c) C.-R. Li, S.-L. Li, X.-M. Zhang, *Cryst. Growth Des.* **2009**, *9*, 1702–1707; d) J. Jiang, F. Gándara, Y.-B. Zhang, K. Na, O. M. Yaghi, W. G. Klemperer, *J. Am. Chem. Soc.* **2014**, *136*, 12844–12847; e) Q. Zhang, S. Dong, P. Shao, Y. Zhu, Z. Mu, D. Sheng, T. Zhang, X. Jiang, R. Shao, Z. Ren, *Science* **2022**, *378*, 181–186.

[15] M. B. Chambers, X. Wang, L. Ellezam, O. Ersen, M. Fontecave, C. Sanchez, L. Rozes, C. Mellot-Draznieks, *J. Am. Chem. Soc.* **2017**, *139*, 8222–8228.

[16] a) S. Han, Y. Huang, T. Watanabe, S. Nair, K. S. Walton, D. S. Sholl, J. C. Meredith, *Microporous Mesoporous Mater.* **2013**, *173*, 86–91; b) S. Han, Y. Huang, T. Watanabe, Y. Dai, K. S.

Walton, S. Nair, D. S. Sholl, J. C. Meredith, *ACS Comb. Sci.* **2012**, *14*, 263–267.

[17] a) M. Sadakiyo, T. Yamada, K. Honda, H. Matsui, H. Kitagawa, *J. Am. Chem. Soc.* **2014**, *136*, 7701–7707; b) X.-M. Li, L.-Z. Dong, S.-L. Li, G. Xu, J. Liu, F.-M. Zhang, L.-S. Lu, Y.-Q. Lan, *ACS Energy Lett.* **2017**, *2*, 2313–2318; c) H. Furukawa, F. Gandara, Y.-B. Zhang, J. Jiang, W. L. Queen, M. R. Hudson, O. M. Yaghi, *J. Am. Chem. Soc.* **2014**, *136*, 4369–4381; d) P. Küsgens, M. Rose, I. Senkovska, H. Fröde, A. Henschel, S. Siegle, S. Kaskel, *Microporous Mesoporous Mater.* **2009**, *120*, 325–330.

[18] a) X. Qian, L. Chen, L. Yin, Z. Liu, S. Pei, F. Li, G. Hou, S. Chen, L. Song, K. H. Thebo, *Science* **2020**, *370*, 596–600; b) I. Riess, *Solid State Ionics* **1996**, *91*, 221–232; c) K. Jiang, T. Fei, F. Jiang, G. Wang, T. Zhang, *Sens. Actuators B* **2014**, *192*, 658–663.

[19] M. Bursch, J. M. Mewes, A. Hansen, S. Grimme, *Angew. Chem. Int. Ed.* **2022**, *61*, e202205735.

[20] H. Yuan, N. Li, W. Fan, H. Cai, D. Zhao, *Adv. Sci.* **2022**, *9*, 2104374.

Manuscript received: April 28, 2023
Accepted manuscript online: June 8, 2023
Version of record online: ■■, ■■

Communications

Metal-Organic Frameworks

W.-H. Deng, Q.-H. Li, J. Chen, C.-Z. Wang, Z.-H. Fu, X.-L. Ye, G.-E Wang, G. Xu* e202305977

A Humidity-Induced Large Electronic Conductivity Change of 10^7 on a Metal-Organic Framework for Highly Sensitive Water Detection

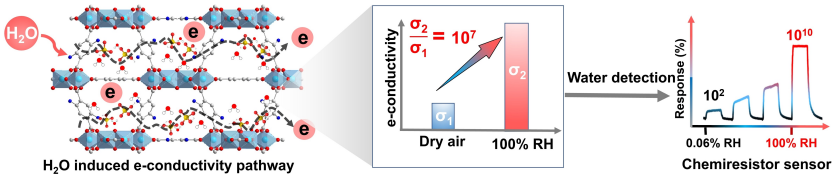

A water-induced large electronic conductivity change of 10^7 on H_2SO_4@$(NH_2)_2$-MIL-125 was observed. Brønsted acid–base pairs formed with the $-NH_2$ groups, and H_2SO_4 played an important role in regulating the conductivity. Based on H_2SO_4@$(NH_2)_2$-MIL-125, a high-performance chemiresistive humidity sensor was developed with the highest sensitivity, broadest detection range and lowest limit of detection amongst all the reported sensing materials to date.